Different Mechanisms of Ca^{2+} Transport in NMDA and Ca^{2+}-permeable AMPA Glutamate Receptor Channels

Lonnie P. Wollmuth and Bert Sakmann

From the Abteilung Zellphysiologie, Max-Planck-Institut für Medizinische Forschung, D-69120 Heidelberg, Germany

abstract   The channel of the glutamate N-methyl-D-aspartate receptor (NMDAR) transports Ca^{2+} approximately four times more efficiently than that of Ca^{2+}-permeable α-amino-3-hydroxy-5-methyl-4-isoxazolepropionate receptors (AMPAR). To investigate the basis of this difference in these glutamate receptors (GluRs), we measured the ratio of Cs$^+$ efflux and Ca^{2+} influx in recombinant NMDAR and Ca^{2+}-permeable AMPAR channels expressed in human embryonic kidney 293 (HEK 293) cells over a wide voltage range. At any one potential, this biionic flux ratio was measured by quantifying the total charge and the charge carried by Ca^{2+} using whole-cell currents and fluorometric techniques (dye overload) with Cs$^+$ internally and Ca^{2+} externally (1.8 or 10 mM) as the only permeant ions. In AMPAR channels, composed of either GluR-A(Q) or GluR-B(Q) subunits, the biionic flux ratio had a biionic flux-ratio exponent of 1, consistent with the prediction of the Goldman-Hodgkin-Katz current equation. In contrast, for NMDAR channels composed of NR1 and NR2A subunits, the biionic flux-ratio exponent was ~2, indicating a deviation from Goldman-Hodgkin-Katz. Consistent with these results, in NMDAR channels under biionic conditions with high external Ca^{2+} and Cs$^+$ as the reference ions, Ca^{2+} permeability (P_{Ca}/P_{Cs}) was concentration dependent, being highest around physiological concentrations (1–1.8 mM; $P_{Ca}/P_{Cs} \approx 6.1$) and reduced at both higher (110 mM; $P_{Ca}/P_{Cs} \approx 2.6$) and lower (0.18 mM; $P_{Ca}/P_{Cs} \approx 2.2$) concentrations. P_{Ca}/P_{Cs} in AMPAR channels was not concentration dependent, being around 1.65 in 0.3–110 mM Ca^{2+}. In AMPAR and NMDAR channels, the Q/R/N site is a critical determinant of Ca^{2+} permeability. However, mutant AMPAR channels, which had an asparagine substituted at the Q/R site, also showed a biionic flux-ratio exponent of 1 and concentration-independent permeability ratios, indicating that the difference in Ca^{2+} transport is not due to the amino acid residue located at the Q/R/N site. We suggest that the difference in Ca^{2+} transport properties between the glutamate receptor subtypes reflects that the pore of NMDAR channels has multiple sites for Ca^{2+}, whereas that of AMPAR channels only a single site.

key words: Ussing flux-ratio test • Goldman-Hodgkin-Katz current equation • Ca^{2+} permeation • fractional Ca^{2+} currents

INTRODUCTION

N-methyl-D-aspartate receptors (NMDAR)[1] and α-amino-3-hydroxy-5-methyl-4-isoxazolepropionate receptors (AMPAR) mediate fast excitatory neurotransmission in the mammalian central nervous system. Post-synaptic influx of Ca^{2+} via glutamate receptors (GluR) is thought to be a critical step for the induction of long-term changes in synaptic strength and neurotoxicity (Choi, 1988; Bliss and Collingridge, 1993). Native NMDAR channels are heteromers composed of the constitutive NR1 subunit and one or more of four different NR2 subunits (A, B, C, D; for review, see Hollmann and Heinemann, 1994). All NMDAR subtypes are, with small quantitative differences, highly permeable to Ca^{2+} (Monyer et al., 1994; Burnashev et al., 1995; Schneggenburger, 1996). In contrast, AMPAR subtypes are more diverse in their ability to transport Ca^{2+} (Hollmann et al., 1991; Hume et al., 1991; Burnashev et al., 1992a; for review, see Burnashev, 1996). Four different AMPAR subunits have been cloned: GluR-A, -B, -C, and -D (alternatively, GluR1-4) (Hollmann and Heinemann, 1994). Ca^{2+}-impermeable AMPAR channels contain the edited form of the GluR-B subunit, termed GluR-B(R), which contains an arginine (R) at the functionally critical Q/R site. AMPAR channels containing only the GluR-A, -C, or -D subunits, which contain a glutamine (Q) at this position, are Ca^{2+} permeable. In NMDAR channels, the homolo-

Lonnie P. Wollmuth's present address is Department of Neurobiology and Behavior, State University of New York at Stony Brook, Stony Brook, NY 11794-5230.

Address correspondence to Dr. Lonnie P. Wollmuth, Department of Neurobiology and Behavior, State University of New York at Stony Brook, Stony Brook, NY 11794-5230. Fax: 516-632-6661; E-mail: lwollmuth@brain.neurobio.sunysb.edu

[1]*Abbreviations used in this paper:* AMPAR, α-amino-3-hydroxy-5-methyl-4-isoxazolepropionate receptor; GHK, Goldman-Hodgkin-Katz; GluR, glutamate receptor; HEK 293 cell, human embryonic kidney 293 cell; I-V, current–voltage; NMDAR, N-methyl-D-aspartate receptor; NMDG, N-methyl-D-glucamine.

gous position to the Q/R site, the N site, is occupied by an asparagine (N) that also contributes to Ca^{2+} transport (Burnashev et al., 1992b).

NMDAR and Ca^{2+}-permeable AMPAR channels show a high but not exclusive selection of Ca^{2+} over monovalent alkali cations. The inward current that the open channel mediates under physiological conditions is carried by a mixture of monovalent (Na^+ and K^+) and Ca^{2+} ions (MacDermott et al., 1986; Mayer and Westbrook, 1987). Recently, a method has been developed using Ca^{2+} photometry and high concentrations of intracellular fura-2 (dye overload), which allows the fraction of the total current carried by Ca^{2+} to be quantified over a wide voltage range (for review, see Neher, 1995). The NMDAR and Ca^{2+}-permeable AMPARs show a quantitative difference in their fractional Ca^{2+} currents (Schneggenburger et al., 1993; Burnashev et al., 1995). For example, at -60 mV and in 1.8 mM Ca^{2+}, recombinant NMDAR channels composed of the NR1–NR2A subunits carry a fractional Ca^{2+} current of $\sim$11%, whereas, for Ca^{2+}-permeable AMPAR, it is $\sim$3% (Burnashev et al., 1995). NMDAR channels also have a higher Ca^{2+} permeability as assessed under biionic conditions than Ca^{2+}-permeable AMPAR channels (e.g., Burnashev et al., 1995).

The mechanism of Ca^{2+} transport in GluR channels remains unclear. Since current amplitudes at any one potential are a balance between inward- and outward-directed currents, understanding mechanisms of ion permeation would be facilitated by defining the properties of the pores that control unidirectional currents over a wide voltage range. Such measurements are typically made only at the zero current or reversal potential, where the inward- and outward-directed currents are exactly balanced, yielding no net current. Although such reversal potential measurements can provide insights into permeation mechanisms (see Hille, 1992), they are limited in that they give information only at a single potential. Alternatively, measurements of unidirectional fluxes at potentials other than the reversal potential have been made using a radioactive tracer on one side of the membrane to distinguish the fluxes. This approach, based on the Ussing flux-ratio test (Ussing, 1949), has been used for voltage-gated K^+ channels using ^{42}K (Hodgkin and Keynes, 1955; Horowicz et al., 1968; Begenisich and De Weer, 1980; Vestergaard-Bogind et al., 1985; Stampe and Begenisich, 1996), and for voltage-gated and amiloride-sensitive Na^+ channels using ^{22}Na and/or ^{24}Na (Begenisich and Busath, 1981; Benos et al., 1983). While this approach has the advantage of examining unidirectional fluxes over a wide potential range, it has the disadvantage of requiring the use of radioactive tracers and therefore has not been extensively used, especially with recombinant ion channels.

To compare the mechanism of Ca^{2+} transport in different GluR channels, we measured at a fixed potential total charge and the charge carried by Ca^{2+} using dye overload with Cs^+ intracellularly and Ca^{2+} extracellularly as the only permeant ions. This allowed us to quantify unidirectional Cs^+ and Ca^{2+} fluxes over a wide voltage range. This approach is comparable with, but not identical to, the Ussing flux-ratio test, which requires that the ion species on both sides of the membrane be the same (see MATERIALS AND METHODS and DISCUSSION). We find that in NMDAR channels the biionic flux ratio of Cs^+ efflux to Ca^{2+} influx shows a strong deviation from the prediction of the Goldman-Hodgkin-Katz (GHK) current equation with a biionic flux-ratio exponent of $\sim$2. In contrast, Ca^{2+}-permeable AMPA channels show no such deviation having a biionic flux-ratio exponent of 1. This difference between GluR channels is not due to the amino acid residue at the Q/R/N site. Thus, the mechanism underlying Ca^{2+} transport in the two types of GluRs is different, and this may be due to differences in the amino acid composition of the external vestibule.

MATERIALS AND METHODS

Heterologous Expression of GluR Channels

All experiments were performed with previously described expression constructs for wild-type NR1–NR2A NMDAR subunits (Wollmuth et al., 1996) and AMPAR subunits (Burnashev et al., 1992a). AMPAR subunits were identified following the nomenclature of Seeburg (1993), with the amino acid residue occupying the Q/R site indicated in parenthesis. Channels were expressed transiently [NR1-NR2A, GluR-B(N)] or permanently [GluR-A(Q), GluR-B(Q)] in human embryonic kidney 293 (HEK 293) cells. All AMPAR channels were of the flip-splice variant form.

Solutions

Intracellular. The standard intracellular solution used to measure fractional Ca^{2+} currents consisted of (mM): 140 CsCl, 10 HEPES, and 2 mM K_5·fura-2, pH adjusted to 7.2 with CsOH. The total intracellular monovalent concentration, $[M]_i$, was 153.5 mM. In measuring Ca^{2+} reversal potentials, the solution was the same except that 10 mM BAPTA replaced the fura-2 ($[M]_i = 163.5$). HEPES and EGTA were obtained from Carl Roth (Karlsruhe, Germany) and BAPTA and fura-2 from Molecular Probes (Eugene, OR).

Extracellular. Fractional Ca^{2+} currents were measured using an extracellular solution consisting of (mM): 1.8 $CaCl_2$, 140 NaCl, and 10 HEPES, pH adjusted to 7.2 with NaOH. To measure fractional Ca^{2+} currents in "pure" extracellular Ca^{2+}, 1.8 or 10 mM Ca^{2+} was added to the following N-methyl-D-glucamine (NMDG)–based solution (mM): 140 NMDG and 10 HEPES, pH adjusted to 7.2 with HCl. The high Cs^+ solution used as a reference to quantify Ca^{2+} permeation consisted of (mM): 140 CsCl and 10 HEPES, pH adjusted to 7.2 with CsOH ($[M]_o = 143.5$). The high Ca^{2+} solution consisted of (mM): 108 $CaCl_2$, 2 $Ca(OH)_2$, and 10 HEPES, with the final pH 7.2. For other Ca^{2+} concentrations, the relevant Ca^{2+} concentration (0.18–10 mM)

was added to the NMDG-based solution. For AMPAR channels, we used 15 μM cyclothiazide to reduce channel desensitization. Two stock solutions of cyclothiazide were used: for all extracellular solutions containing monovalents, the stock solution was 10 mM cyclothiazide dissolved in 100 mM NaOH. Alternatively, for solutions containing Ca^{2+} and NMDG, 0.5 mM cyclothiazide was dissolved in (mM): 10 $Ca(OH)_2$, 140 NMDG, and 10 HEPES. Appropriate amounts of 140 mM NMDG and 10 mM HEPES and $CaCl_2$ were mixed, along with this stock solution, to yield the final Ca^{2+} concentration indicated in the text.

Current Recordings and Data Analysis

Currents were recorded at room temperature (20–23°C) using an EPC-9 amplifier with PULSE software (HEKA Elektronik, Lambrecht, Germany), low pass filtered at 500 Hz, and digitized at 2 kHz. Pipettes were pulled from borosilicate glass and had resistances of 0.8–3 MΩ when filled with the pipette solution and measured in the Cs^+ external solution. External solutions were applied using a piezo-driven double-barrel application system. For NMDAR channels, one barrel contained the external solution plus 50 μM glycine, and the other barrel the same solution but with added 200 μM glutamate. For AMPAR channels, one barrel contained the external solution plus 15 μM cyclothiazide and the other barrel the same solution but with added 1 mM glutamate. The liquid-junction potential between the CsCl pipette solution and the 143.5 mM Cs^+ and 143.5 mM Na^+ external solutions was −0.9 and −1.6 mV, respectively (pipette negative). Ca^{2+}-containing solutions generated junction potentials between the ground electrode and high CsCl solution of −10.1 (0.18–1.8 mM $CaCl_2$ in NMDG), −10.5 mV (10 mM $CaCl_2$ in NMDG), and −10.2 mV (110 mM $CaCl_2$) (ground electrode 0 mV). All curve fitting was done using Igor Pro (WaveMetrics, Inc., Lake Oswego, OR). Results are reported in the text as mean ± SEM and shown graphically as mean ± 2*SEM.

Fluorescence Measurement

Fura-2 (2 mM) was loaded into HEK 293 cells via the patch pipette to measure the fraction of the total current (monovalents and Ca^{2+}) carried by Ca^{2+} (see Neher, 1995). Cells were illuminated alternatively at 365 and 385 nm (2–10 Hz) by a polychromatic illumination system (T.I.L.L. Photonics, München, Germany). Excitation light was coupled to the microscope via a light guide and was attenuated to 90–95% with neutral density filters. A 425-nm dichroic mirror and a 500–530-nm band-pass emission filter were included in the light path. Fluorescence signals were measured with a photomultiplier (Luigs and Neumann, Ratingen, Germany). Changes in $[Ca^{2+}]_i$ were estimated from the fluorescence signals according to Grynkiewicz et al. (1985).

Fractional Ca^{2+} currents were measured according to Burnashev et al. (1995) and Neher (1995). In brief, the decrement in fura-2 fluorescence at 385-nm excitation (ΔF_{385}) evoked by a Ca^{2+} influx depends on the relative Ca^{2+}-binding ratio of exogenous (κ'_B) and endogenous (κ_S) buffers:

$$\Delta F_{385} = \Delta F_{max} \frac{\kappa'_B}{1 + \kappa_S + \kappa'_B}.$$

In the case of overload, that is when the fura-2 Ca^{2+}-binding ratio is much greater than the Ca^{2+}-binding ratio of the endogenous buffer ($\kappa'_B \gg \kappa_S$). the decrement approaches the maximal value, ΔF_{max}, which is directly proportional to the total Ca^{2+} influx:

$$\Delta F_{385} = \Delta F_{max} = f_{max} Q_{Ca} \qquad (\kappa'_B \gg \kappa_S). \qquad (1)$$

The proportionality constant, f_{max}, also termed maximal F/Q ratio (Schneggenburger et al., 1993), between the charge carried by inward Ca^{2+} (Q_{Ca}) and ΔF_{385} was determined as outlined below. The overload approach to quantifying Ca^{2+} influx requires that all of the incoming Ca^{2+} is captured by fura-2 rather than by endogenous buffers. The duration of the glutamate application at any one potential therefore was chosen such that $[Ca^{2+}]_i$ remained below 200 nM. Also, in instances where Ca^{2+} was the only external permeant ion, we held the cells at −10 or 0 mV, leading to a low resting $[Ca^{2+}]_i$ of ∼10–50 nM. In any case, even under extreme conditions beyond those used in this study (e.g., resting $[Ca^{2+}]_i$ of 100 nM and a peak $[Ca^{2+}]_i$ of 300 nM), the Ca^{2+}-binding ratio, κ'_B, of 2 mM fura-2 (2,660; derived using Eq. 28 in Neher, 1995) still far exceeds the endogenous Ca^{2+}-binding ratio, κ_S, of HEK 293 cells (≈50; Burnashev et al., 1995). To verify this assumption, we also measured the derived parameter, abs(Q_{Cs}/Q_{Ca}) (see Figs. 3–5), at a single voltage (−21 mV) over a range of Q_{Ca} (Fig. 1 C). This parameter was independent of the amount of Ca^{2+} influx, confirming the idea that dye depletion was not a significant problem even up to 140 pC.

Fractional Ca^{2+} currents (P_f) were quantified using the relationship:

$$P_f(\%) = 100 \frac{f}{f_{max}} = 100 \frac{\Delta F_{385}}{Q_T \cdot f_{max}} \frac{1}{BU}. \qquad (2)$$

To account for instabilities of the illumination intensity or the detection efficiency, ΔF_{385} was normalized to the fluorescence of beads (4.5-μm-diameter fluoresbrite BB beads, Lot 460565; Polysciences Inc., Warrington, PA) and expressed in "bead units" (BU; Schneggenburger et al., 1993). The bead unit was determined on each experimental day as the mean fluorescence of 8–15 beads at 385-nm excitation. Fluorescent measurements were made only on small cells (<6 pF) that were either attached or lifted. Green fluorescent protein was cotransfected to detect transfected cells, but this fluorescent marker has no effect on P_f measurements (Schneggenburger, 1996).

The proportionality constant, f_{max}, which needs to be measured under conditions where the total charge (Q_T) ≈ Q_{Ca} was quantified in two ways. (a) For NMDAR channels, ΔF_{385} at −100 mV was measured with Cs^+ intracellularly and, with 10 mM Ca^{2+}, 140 mM NMDG extracellularly. The total amount of charge at this potential, which was assumed to be carried by Ca^{2+}, was varied by altering the length of the glutamate application (typically 100–1,000 ms) (Fig. 1 A). The f_{max} was derived from the slope of a fitted line to a plot of ΔF_{385} against Q_T and was 1.22 ± 0.05 $BU/$ nC ($n = 5$) (Fig. 1 B). We also measured f_{max} using the same approach at −80 and −60 mV (Fig. 1 B); these values were not significantly different from that measured at −100 mV, confirming the idea that the total current at −100 mV is carried almost exclusively by Ca^{2+}. (b) The second approach to quantify f_{max} followed that of Schneggenburger (1996). In brief, reversal potential shifts on adding Ca^{2+} (1.8 or 10 mM) to a Ca^{2+}-free solution (143.5 mM NaCl) were used to estimate the monovalent reversal potential in Ca^{2+}-containing solutions during P_f measurements. Assuming independence of ion movement, the f ratio (or F/Q ratio) at the monovalent reversal potential should solely be due to Ca^{2+} influx. For NR1–NR2A channels in 1.8 mM Ca^{2+}, this approach yielded an f_{max} of 1.00 ± 0.02 $BU/$nC ($n = 3$), significantly less than that measured using approach a. Based on our measured f ratios for NR1–NR2A channels at −60 mV in 1.8 mM Ca^{2+}, this f_{max} would yield a P_f of ∼16.5%, comparable to the value measured by Schneggenburger (1996). Approach b was also used for GluR-B(N) channels, which are mutant GluR-B channels containing an asparagine at the Q/R site. These channels were selected since they are Ca^{2+} permeable but are not

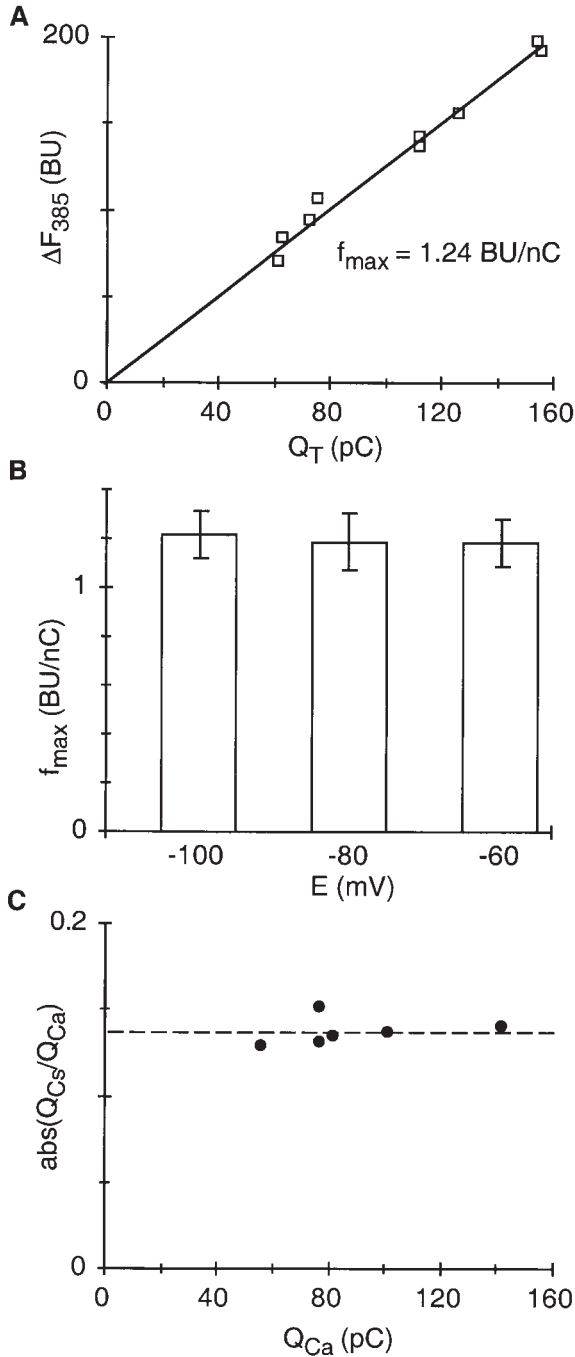FIGURE 1. Determination of f_{max} in NR1-NR2A NMDAR channels in high external Ca^{2+}. (*A*) ΔF_{385} plotted against the total charge (Q_T) recorded at -100 mV in a HEK 293 cell expressing NR1-NR2A channels. The cell was bathed in 10 mM Ca^{2+}, 140 mM NMDG. Values were derived like those shown in Fig. 3. Variations in Q_T were produced by varying the length of the glutamate application from 100 to 1,000 ms. The solid line is a fitted linear equation. (*B*) Average f_{max} ($\pm 2*SEM$) determined as in *A* at -100, -80, and -60 mV. The total number of recordings was, from left to right, 5, 4, and 4. (*C*) The derived parameter, abs(Q_{Cs}/Q_{Ca}), plotted against Ca^{2+} influx recorded at -21 mV in a HEK 293 cell expressing NR1-NR2A channels (same cell as in Fig. 3). See Figs. 3–5 for details on the derivation of abs(Q_{Cs}/Q_{Ca}). Variations in Q_T were

blocked by intracellular polyamines, allowing currents to be readily measured around the reversal potential. For GluR-B(N) channels, f_{max} was 1.30 ± 0.02 *BU*/nC ($n = 5$) in 1.8 mM Ca^{2+} and 1.25 ± 0.03 *BU*/nC ($n = 4$) in 10 mM Ca^{2+}. For NR1–NR2A channels, this f_{max} would yield a P_f at -60 mV (1.8 mM Ca^{2+}) of $\sim 13\%$, comparable to values obtained elsewhere for recombinant (Burnashev et al., 1995) and native (Rogers and Dani, 1995) NMDAR channels. We used as an f_{max} value a grand mean (1.26 ± 0.02 *BU*/nC) of those values derived from approaches *a* and *b* for GluR-B(N) channels for the following reasons: first, they yielded comparable values and, second, independence of ionic movement is a fundamental assumption of approach *b*, but our results suggest that this assumption is violated in NMDAR but not in GluR-B(N) channels.

Biionic Flux Ratios

The Ussing (1949) flux-ratio equation relates the unidirectional fluxes, ϕ_{efflux} and ϕ_{influx}, for passive, independent movement of a single ion species across the membrane:

$$\frac{\phi_{efflux,S}}{\phi_{influx,S}} = \frac{[S]_i}{[S]_o}\exp\left(\frac{z_S E}{RT/F}\right),$$

where $[S]_i$ and $[S]_o$ are the concentration of ion species *S* on the intracellular and extracellular side of membrane, respectively, and z_S its valence. *R, T,* and *F* have their normal meanings, and the quantity RT/F was 25.4 mV (21°C). This equation is valid when the intracellular and extracellular ions are the same. However, in our case, we are interested in determining the unidirectional flux ratios for ions having different valence, namely the efflux of a monovalent ion (Cs^+) and the influx of a divalent ion (Ca^{2+}). As a theoretical approach to describe these ratios, we started with the unidirectional current components of the GHK current equation (see Hille, 1992):

$$\frac{I_{efflux,S}}{I_{influx,S}} = \frac{Q_{Cs}}{Q_{Ca}} = \frac{P_{Cs}}{P_{Ca}}\frac{[Cs^+]_i}{[Ca^{2+}]_o}\frac{1-\exp\left(\frac{2E}{RT/F}\right)}{1-\exp\left(\frac{-E}{RT/F}\right)}, \quad (3)$$

where Q_{Cs} and Q_{Ca} are the total charge carried by Cs^+ and Ca^{2+} during a specific time interval. At any one potential, Q_T and Q_{Ca} ($= \Delta F_{385}/f_{max}$, Eq. 1) were quantified over the same time interval. Q_{Cs} was derived using the relationship, $Q_T = Q_{Ca} + Q_{Cs}$. The quantity, Q_{Cs}/Q_{Ca}, is not a proper flux ratio since the ions have a different valence. Therefore, we refer to it as a biionic flux ratio to distinguish it from an Ussing type flux ratio. To compare results under different ionic conditions, we expressed Eq. 3 relative to the zero current or reversal potential ($E_{rev,Ca}$) for Ca^{2+}. Using the Lewis equation (see Eq. 7), Eq. 3 was expressed relative to $E_{rev,Ca}$:

$$\frac{Q_{Cs}}{Q_{Ca}} = \frac{1}{\exp\left(\frac{E_{rev,Ca}}{RT/F}\right)+\exp\left(\frac{2E_{rev,Ca}}{RT/F}\right)}\frac{1-\exp\left(\frac{2E}{RT/F}\right)}{1-\exp\left(-\frac{E}{RT/F}\right)}. \quad (4)$$

For simplicity, we define the right hand part of Eq. 4 as Λ.

produced by varying the length of the glutamate application from 100 to 1,000 ms.

The assumptions underlying the derivation of Eq. 4 do not apply generally. In instances where Eq. 4 does not hold, we found it useful to use the following empirical expression:

$$\frac{Q_{Cs}}{Q_{Ca}} = \Lambda^{n'}, \qquad (5)$$

where Eq. 4 is raised to some power, n', denoted the biionic flux-ratio exponent. Eq. 5 has a formal similarity to the Ussing type flux-ratio exponent, but the mechanistic interpretation of n' is obscure. We use it as a short-hand notation to indicate deviations from Eq. 4. At any one potential, it was quantified by solving for n':

$$n' = \frac{\ln(Q_{Cs}/Q_{Ca})}{\ln(\Lambda)}. \qquad (6)$$

This approach to quantifying the biionic flux ratio requires that the only permeant ions are Cs^+ intracellularly and Ca^{2+} extracellularly. To generate a pure Ca^{2+}-containing solution, we added various concentrations of Ca^{2+} to 140 mM NMDG. NMDG is impermeant in NMDAR channels (Villarroel et al., 1995). On the other hand, Ca^{2+}-permeable AMPAR channels show a weak NMDG permeability. For GluR-A(Q) channels, P_{NMDG}/P_{Cs} is ~0.02 (Burnashev et al., 1996), whereas it is ~0.01 in GluR-B(Q) and essentially impermeant in GluR-B(N) (N. Burnashev, personal communication). To avoid any contamination by NMDG in GluR-A(Q) and GluR-B(Q) channels, we measured the biionic flux ratio only in 10 mM $[Ca^{2+}]_o$, where any contribution of an NMDG current component would be small.

Ca^{2+} Reversal Potentials

To quantify Ca^{2+} permeability from reversal potential measurements, we started with the Lewis equation (Lewis, 1979), which takes into account the presence of multiple permeant ions having different valences. With Cs^+ as the only permeant ion intracellularly, this equation has the form:

$$E_{rev} = \frac{RT}{F}\ln\frac{[Cs^+]_0 + \frac{P_{mono}}{P_{Cs}}[mono]_0 + 4\frac{P'_{Ca}}{P_{Cs}}[Ca^{2+}]_0}{[Cs^+]_i}, \qquad (7)$$

where P_{mono}/P_{Cs} is the permeability ratio of any other permeant monovalent species, and P'_{Ca} is $P_{Ca}/[1 + \exp(E_{rev}F/RT)]$. Ca^{2+} permeability was determined by measuring the change of reversal potential (ΔE_{rev}) for glutamate-activated currents on replacing 143.5 mM Cs^+ with a pure Ca^{2+} solution (0.18–10 mM Ca^{2+} in NMDG or 110 mM Ca^{2+}). Permeability ratios, P_{Ca}/P_{Cs}, were calculated according to the relation:

$$E_{rev,Ca} - E_{rev,Cs} = \frac{RT}{F}\ln\frac{4\frac{P_{Ca}}{P_{Cs}}[Ca^{2+}]_0}{[Cs^+]_0\left[1 + \exp\left(\frac{E_{rev,Ca}}{RT/F}\right)\right]}, \qquad (8)$$

where $E_{rev,Ca}$ is the reversal potential in the Ca^{2+}-containing solution, and $E_{rev,Cs}$ is the reversal potential in the reference Cs^+-containing solution. For simplicity, we present throughout the manuscript only Ca^{2+} concentrations. We also calculated P_{Ca}/P_{Cs} using activity coefficients (i.e., concentrations in Eq. 8 were multiplied by γ, the activity coefficient). Mean molal activity coefficients were found in the NIST Standard Reference Database 44 (U.S. Department of Commerce, Washington, DC); individual activity coefficients were, following the Guggenheim convention, γ_{Ca} 0.26 (110 mM Ca^{2+}), 0.30 (10 mM Ca^{2+}) and 0.31

(0.18–1.8 Ca^{2+}), and γ_{Cs} 0.72 (143.5 mM Cs^+). Because these activity coefficients were not greatly different (Ca^{2+} was present in high concentrations of NMDG), they increased the magnitude of P_{Ca}/P_{Cs} approximately equally over the entire concentration range (data not shown). In most instances, the control recording was an average of the control recording made before and after exposure to the Ca^{2+}-containing solution.

Measuring flux ratios requires quantifying the unidirectional movement of ions in a channel at a fixed membrane potential. To do so in GluR channels, we simultaneously measured whole-cell currents by voltage clamp and Ca^{2+} influx with fluorescence under ionic conditions where Cs^+ internally and Ca^{2+} externally were the only permeant ions. Under such conditions, the total charge during a defined time interval (Q_T) is carried by inward moving Ca^{2+} and outward moving Cs^+ (i.e., $Q_T = Q_{Ca} + Q_{Cs}$). The unidirectional Q_{Cs} component was derived as $Q_T - Q_{Ca}$. We refer to the quantity Q_{Cs}/Q_{Ca} as a biionic flux ratio (see MATERIALS AND METHODS).

Unidirectional Currents in NR1-NR2A NMDAR Channels

Fig. 2, *A* and *B*, shows whole-cell glutamate-activated currents in a HEK 293 cell expressing NR1-NR2A channels. The cell was bathed either in 143.5 mM Cs^+ (*A*) or in 10 mM Ca^{2+}, 140 mM NMDG (*B*) with the pipette solution always containing 163.5 mM Cs^+. The current–voltage (I-V) relation of the corresponding peak currents is shown in Fig. 2 *C*. The currents in the external Cs^+ solution (○) cross the voltage axis at −3.6 mV, close to the Nernst potential for Cs^+ (−3.3 mV). When Ca^{2+} replaces Cs^+ (●), the I-V relation is strongly outwardly rectifying. However, despite the nearly 14-fold reduction in concentration of a permeant species, the reversal potential is shifted only slightly leftwards, to ~−12 mV. On average, replacing Cs^+ with 10 mM Ca^{2+} produced a shift in the reversal potential of −8.7 ± 0.3 mV ($n = 6$), yielding a mean P_{Ca}/P_{Cs} of 4.2, consistent with Ca^{2+} being more permeant in NMDAR channels than monovalent alkali cations.

The use of fluorometry, in combination with whole-cell current recording, to quantify unidirectional fluxes is shown in Fig. 3. The recordings are from a HEK 293 cell measured in 10 mM Ca^{2+}, 140 mM NMDG, like the cell in Fig. 2 *C* (●), except that 2 mM fura-2 was included in the pipette solution. At such high concentrations, fura-2 captures most of the Ca^{2+} entering the cell (see MATERIALS AND METHODS). Changes in the fluorescence signal at 385 nm excitation are therefore proportional to the total Ca^{2+} influx (Q_{Ca}), with the proportionality constant defined by f_{max} (≈1.26 *BU*/nC; see MATERIALS AND METHODS) according to the relationship $Q_{Ca} = \int I_{Ca}dt = \Delta F_{385}/f_{max}$.

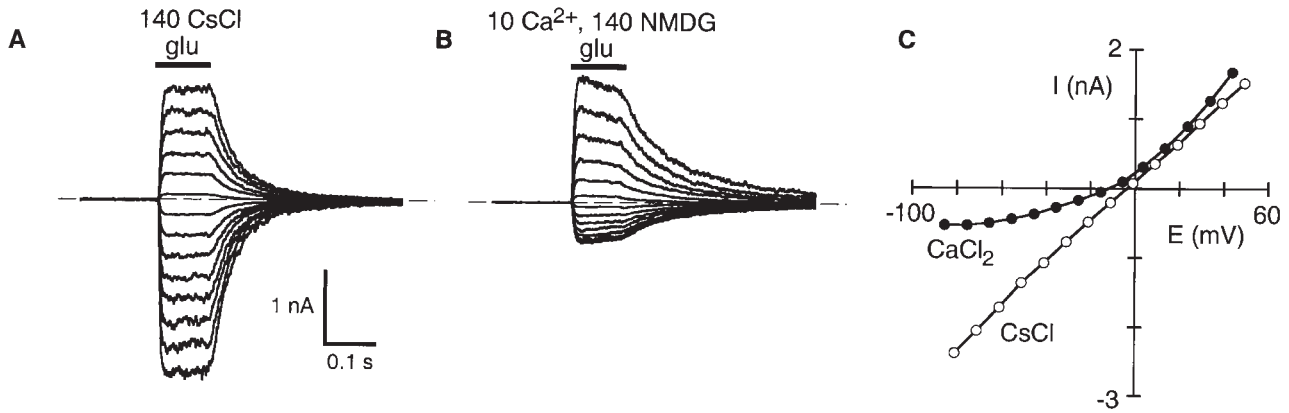Fig. 3 shows recordings from the same cell with the reversal potential ($E_{rev,Ca}$) at −11 mV. At −31 mV (Fig.

FIGURE 2. Ca^{2+} permeation in wild-type NMDAR channels. (*A* and *B*) Glutamate-activated currents at different membrane potentials, in 10-mV increments, in a HEK 293 cell expressing NR1-NR2A channels. The cell was bathed either in 143.5 mM CsCl (*A*) or 10 mM $CaCl_2$, 140 mM NMDG (*B*). The pipette solution contained 163.5 mM CsCl. (*C*) Peak I-V relation for records shown in *A* and *B*. The CsCl record is an average of the currents recorded before and after the $CaCl_2$ recording.
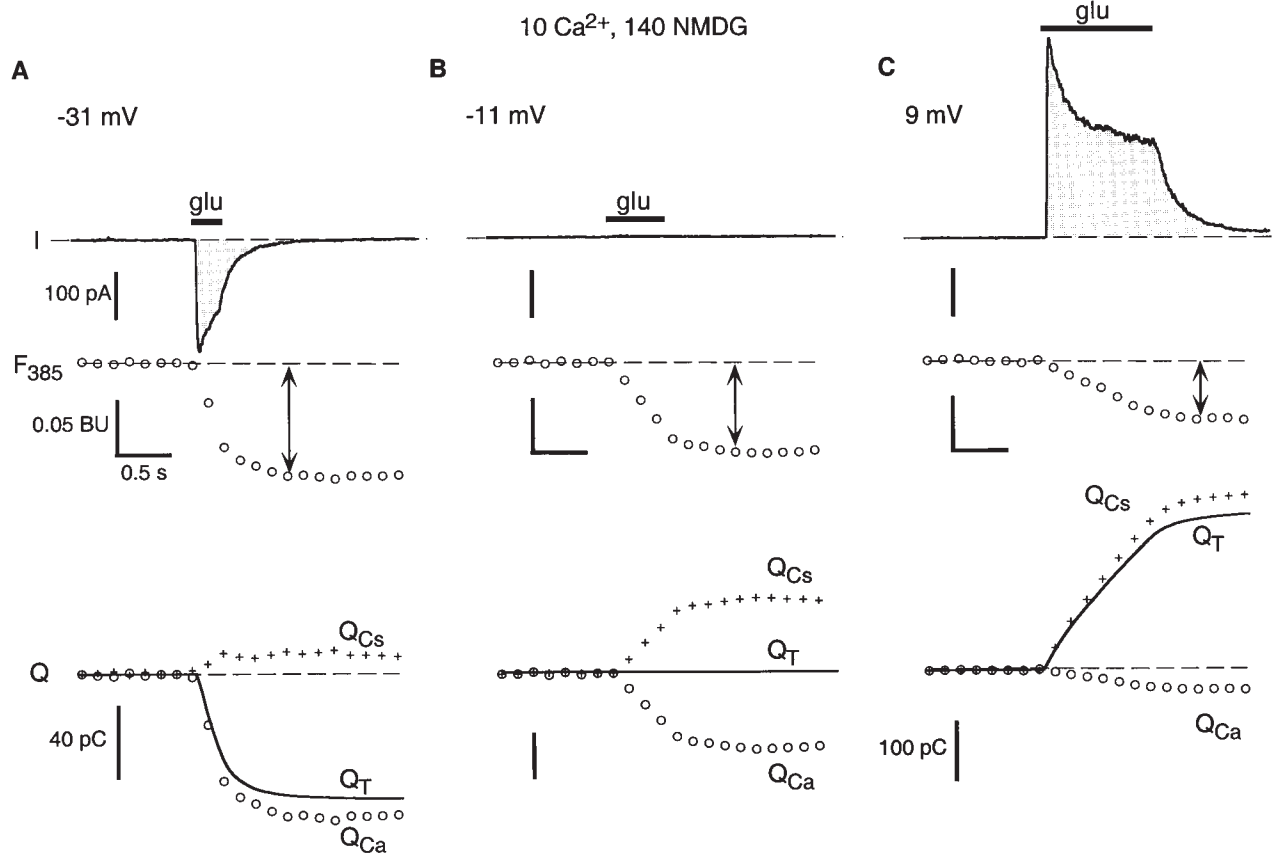

FIGURE 3. Simultaneous measurement of whole-cell current and Ca^{2+} influx in NR1-NR2A NMDAR channels. (*A–C*) Whole-cell current (*I*), fluorescent intensity with 385 nm excitation (F_{385}) and corresponding charge movements (*Q*) evoked by glutamate applications (*solid bars*) at −31 (*A*), −11 (*B*), and +9 (*C*) mV. The recordings are from a HEK 293 cell bathed in 10 mM $CaCl_2$, 140 mM NMDG with the pipette solution containing 143.5 mM CsCl, 2 mM fura-2. In lower traces, Q_T (*solid line*) was derived from the time integral of the whole-cell current. Q_{Ca} (○) was derived from the relationship $Q_{Ca} = \Delta F_{385}/f_{max}$ (see MATERIALS AND METHODS) where ΔF_{385} was taken as the difference between the F_{385} amplitude at each time point and the baseline F_{385} signal (*dashed line*), which was extrapolated from a linear fit to the F_{385} amplitudes before the glutamate application. Q_{Cs} (*pluses*) was derived from the relationship $Q_{Cs} = Q_T − Q_{Ca}$. The double arrows in the F_{385} traces indicate the time point at which Q_{Ca} and Q_T were quantified. The dashed line in each plot reflects the 0 level. Between the current traces shown in the panels, the cell was held at −10 mV. The $[Ca]_i$ before the glutamate application was between 10 and 30 nM. No fast Ca^{2+} clearance mechanism occurring on the time scale of these recordings was present.

3 *A*), which is -20 mV of $E_{rev,Ca}$, the application of glutamate (*solid bar*) yields an inward directed current (trace *I*). As expected, there is also a corresponding decrement in the fluorescence signal at 385 nm excitation (ΔF_{385}), showing that Ca^{2+} flows into the cell. As shown in the *Q* plot (*bottom*), the unidirectional Ca^{2+} influx (Q_{Ca}), derived from the ΔF_{385} measurement, and the total charge (Q_T), derived from the time integral of the whole-cell current, were inwardly directed but not of equal magnitude. With Cs^+ internally and Ca^{2+} externally as the only permeant ions, yielding a net flux less than the influx of Ca^{2+} requires that there be a unidirectional efflux of Cs^+ (Q_{Cs}). The ratio of Q_{Cs} to Q_{Ca} was essentially constant at each time point (data not shown). However, we quantified Q_{Ca} and Q_{Cs} at a single time point typically when F_{385} reached an initial minimum. At the time interval indicated (Fig. 3, *arrow*), Q_T was -66.9 pC and the Ca^{2+} influx was -76.9 pC, yielding an efflux of Cs^+ of $\sim$10 pC. (Like current flows, we assign inward directed charge movements a negative value.)

At -11 mV (Fig. 3 *B*), the application of glutamate (*solid bar*) yields no net current, indicating that this potential represents the reversal potential. There is a large decrement in F_{385}, indicating an influx of Ca^{2+}, which must be exactly balanced by Cs^+ efflux to yield a net zero current (*Q* plot). At $+9$ mV (Fig. 3 *C*), which is $+20$ mV positive to $E_{rev,Ca}$, a longer glutamate application time (1 s) was required since a smaller portion of the total current was carried by Ca^{2+}. At this potential, Q_T was outwardly directed. At the indicated time interval, Q_T was 303 pC. The corresponding Ca^{2+} influx during the same time interval was -38.9 pC, yielding a Cs^+ efflux of 341.9 pC.

Using the methods illustrated in Fig. 3, we quantified in NMDAR channels the unidirectional fluxes of Cs^+ and Ca^{2+} (Fig. 4 *A*), and the corresponding absolute ratio of the unidirectional fluxes, $abs(Q_{Cs}/Q_{Ca})$, over a wide voltage range. For ease of comparison, the values

A
Q (pC)
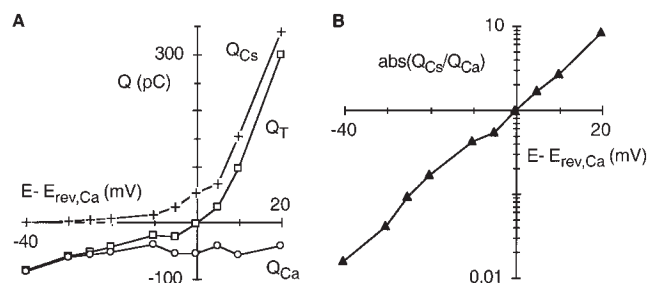300
Q_{Cs}
Q_T
E- $E_{rev,Ca}$ (mV)
20
-40
-100
Q_{Ca}

B
10
$abs(Q_{Cs}/Q_{Ca})$
-40
20
E- $E_{rev,Ca}$ (mV)
0.01

FIGURE 4. Dependence of charge movements on membrane potential. (*A*) Q_T ($\square$), Q_{Ca} ($\bigcirc$), and Q_{Cs} ($+$) plotted relative to the reversal potential. (*B*) Corresponding plot of the absolute of the biionic flux ratio, Q_{Cs}/Q_{Ca}, for the record shown in *A*. Values are plotted relative to the reversal potential.

are plotted relative to the reversal potential ($E - E_{rev,Ca}$). The voltage range over which the unidirectional fluxes was measured was limited at negative potentials since Q_{Ca} approached Q_T (Fig. 4 *A*), making Q_{Cs} small and unreliable. At positive potentials, it was limited since long pulses of glutamate were required to obtain a detectable ΔF_{385} with the baseline F_{385} having to be extrapolated over a long time.

Biionic Flux Ratios in NMDAR Channels Deviate from the Prediction of the GHK Equation

Fig. 5 summarizes the ratio of the unidirectional Cs^+ efflux and Ca^{2+} influx measured either with 10 mM $[Ca^{2+}]_o$ (Fig. 5 *A*) or 1.8 mM $[Ca^{2+}]_o$ (Fig. 5 *B*) in NR1-NR2A channels. As a theoretical basis, we used the unidirectional current components of the GHK current equation to describe these results (Eq. 3). At both concentrations, the biionic flux ratios show a strong deviation from a biionic flux-ratio exponent of 1 (Eq. 3 and Fig. 5, *solid lines*). Indeed, in 10 mM $[Ca^{2+}]_o$ (Fig. 5 *A*), the results were best described using an average biionic flux-ratio exponent of 2.02 ± 0.06 (Eq. 5). This biionic flux-ratio exponent showed no voltage dependence from -40 to $+40$ mV of $E_{rev,Ca}$. In 1.8 mM $[Ca^{2+}]_o$ (Fig. 5 *B*) and from -40 to $+40$ mV of $E_{rev,Ca}$, the biionic flux-ratio exponent was 1.90 ± 0.04, somewhat smaller than that found in 10 mM $[Ca^{2+}]_o$. At very negative potentials, starting at ~ -40 mV of $E_{rev,Ca}$, the biionic flux ratios started to show a weak voltage dependence with the biionic flux-ratio exponent getting smaller. However, at potentials so negative from the reversal potential, the biionic flux ratio was difficult to quantify accurately since Q_{Ca} approached Q_T (see Fig. 4 *A*; a similar problem occurs in 10 mM $[Ca^{2+}]_o$ as seen by the greater variability in biionic flux ratios with negative potentials). Nevertheless, the strong deviation from Eq. 3 at both Ca^{2+} concentrations suggests that Cs^+ efflux and Ca^{2+} influx in NMDAR channels do not follow the GHK equation, and that at least ± 40 mV of the reversal potential, this process is essentially voltage independent.

Biionic Flux Ratios in Ca^{2+}-permeable AMPAR Channels Show a Biionic Flux-Ratio Exponent of 1

Fig. 6 illustrates recordings, comparable to those in Fig. 3, from Ca^{2+}-permeable AMPAR channels assembled from GluR-A(Q) subunits. Fig. 6, *A* and *B*, shows I-V relations for glutamate-activated currents in the presence of cyclothiazide from a HEK 293 cell expressing GluR-A(Q) channels bathed either in CsCl or CaCl₂. (Fig. 6 *B* is the same I-V relation as *A*, but with an expanded current scale.) In Cs^+ ($\square$), the I-V relation shows a strong double rectification due to a voltage-dependent block of Ca^{2+}-permeable AMPAR channels by intracellular polyamines (Bowie and Mayer, 1995; Koh et al., 1995*a*).
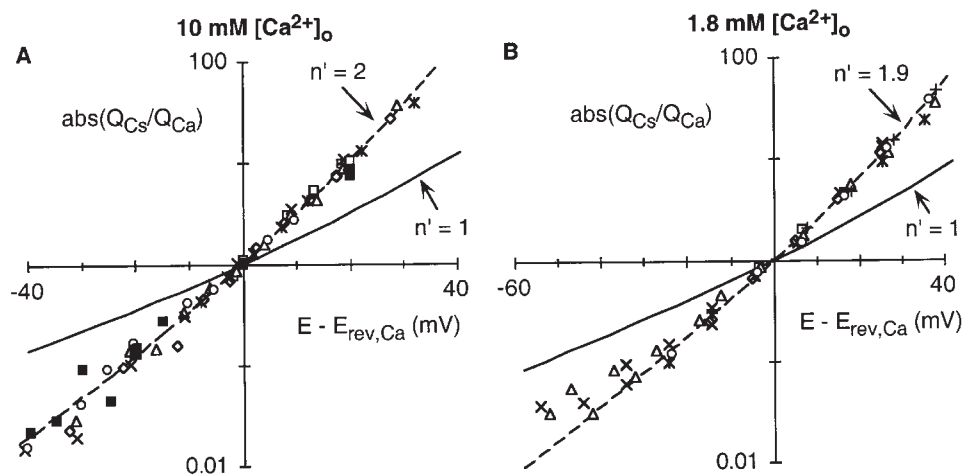
FIGURE 5. Biionic flux ratios in NR1-NR2A NMDAR channels. Absolute of the biionic flux ratio, Q_{Cs}/Q_{Ca}, in NR1-NR2A channels measured in 10 (A) or 1.8 (B) mM CaCl$_2$ in 140 mM NMDG. Values are plotted relative to the reversal potential ($E_{rev,Ca}$). The absolute $E_{rev,Ca}$ was ~-11 (10 Ca^{2+}) and -37(1.8 Ca^{2+}) mV . The same symbols are measurements from the same cell, but different cells were used in A and B (eight different cells were tested at each concentration). Within each individual cell, $E_{rev,Ca}$ was estimated using 2-mV voltage steps. The lines in each plot are Eq. 5 raised to the indicated biionic flux-ratio exponent, n', which was determined from linear fits of n' plotted against $E - E_{rev,Ca}$. For Eq. 5, $E_{rev,Ca}$ was derived from mean P_{Ca}/P_{Cs} shown in Fig. 8.
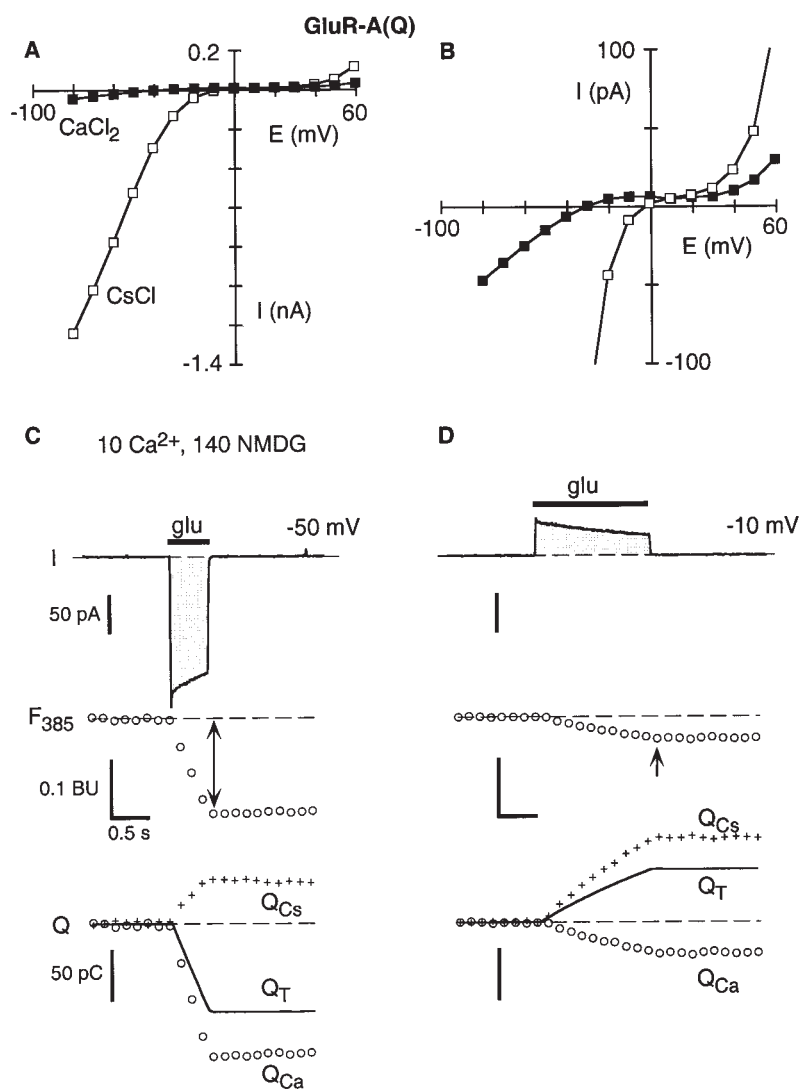

FIGURE 6. Simultaneous measurement of whole-cell current and Ca^{2+} influx in Ca^{2+}-permeable GluR-A(Q) AMPAR channels. (A) Peak I-V relation for glutamate-activated currents, in the presence of 15 μM cyclothiazide, recorded in a HEK 293 cell permanently expressing homomeric GluR-A(Q) channels. Records recorded and displayed as in Fig. 2 C. (B) The same record as in A, but with an expanded current scale. (C and D) Whole-cell current (I) and fluorescent intensity with 385-nm excitation (F_{385}) evoked by glutamate applications at -10 (C) and -50 (D) mV. The scale bars in C apply to both panels. $E_{rev,Ca}$ in this cell was -30 mV (data not shown). Records displayed and analyzed as in Fig. 3.

The currents in the Cs⁺ solution cross the voltage axis near −4 mV. [Because of the strong block by polyamines around 0 mV, we normally used voltage steps in 2-mV increments to quantify the reversal potentials in the CsCl solution, but use Fig. 6, *A* and *B*, to illustrate the overall shape of the I-V relation in GluR-A(Q) channels]. When Ca²⁺ replaces Cs⁺ (■), the I-V relation remains strongly doubly rectifying with the reversal potential shifted leftward to ∼−30 mV. On average, replacing Cs⁺ with 10 mM [Ca²⁺]ₒ in GluR-A(Q) channels produced a shift in the reversal potential of −26.6 ± 0.7 mV ($n = 4$), yielding a mean P_{Ca}/P_{Cs} of 1.60. This result is consistent with Ca²⁺ being more permeant in Ca²⁺-permeable AMPAR channels than monovalent alkali cations, although the relative permeability is less than that in NMDAR channels.

Fig. 6, *C* and *D*, shows simultaneous measurement of whole-cell currents and Ca²⁺ influx, with Cs⁺ internally and 10 mM Ca²⁺ externally, to quantify unidirectional fluxes in GluR-A(Q) channels. In this cell, $E_{rev,Ca}$ is ∼−30 mV (data not shown). At −50 mV (Fig. 6 *C*), the glutamate application in the presence of cyclothiazide elicited a large inwardly directed current. Q_T at the selected time interval (*arrows*) was ∼−88.4 pC. Based on the corresponding ΔF_{385} measurement, inward Ca²⁺ carried −133.4 pC of this charge, yielding a Cs⁺ efflux of 45 pC and an abs(Q_{Cs}/Q_{Ca}) of 0.38, a value larger

than that at the same relative potential found in NMDAR channels (≈0.13, Fig. 3 *A*). At −10 mV (Fig. 6 *D*), the glutamate application resulted in a small outward-directed current. The total charge during the selected time interval was 53.2 pC with inward Ca²⁺ carrying −31.2 pC of this charge, yielding a Cs⁺ efflux of 84.4 pC. The abs(Q_{Cs}/Q_{Ca}) was therefore 2.71, considerably smaller than that for NMDAR channels at the same relative potential (≈8.8, Fig. 3 *C*).

Fig. 7 summarizes the biionic flux ratio for GluR-A(Q) channels (*open symbols*) as well as GluR-B(Q) channels (*solid symbols*) in 10 mM [Ca²⁺]ₒ over a wide voltage range. Because of the strong block by intracellular polyamines of GluR-A(Q) and GluR-B(Q) channels, this ratio could only be measured until ∼30 mV positive to $E_{rev,Ca}$. Nevertheless, in both Ca²⁺-permeable AMPAR channel types, the biionic flux-ratio exponent was 1, following the predictions of the GHK current equation (Fig. 7, *solid line*).

Ca²⁺ Permeability in NMDAR but Not in Ca²⁺-permeable AMPAR Channels Is Concentration Dependent

The results for the biionic flux-ratio experiments suggest that NMDAR but not AMPAR channels deviate from the prediction of GHK. Another indication of such a deviation is a concentration dependence of permeability ratios. To test this possibility, we quantified Ca²⁺ permeability over a wide concentration range of extracellular Ca²⁺ for NMDAR (Fig. 8, *A* and *B*) and Ca²⁺-permeable AMPAR (Fig. 8, *C* and *D*) channels.

Fig. 8 *A* summarizes the change in reversal potential on replacing high Cs⁺ with a wide range of different Ca²⁺ concentrations (0.18–110 mM) in NR1-NR2A channels. The smooth curve was derived using the GHK equation and assuming a P_{Ca}/P_{Cs} of 4.8. The curve does not describe the results well as they fall below it both at very low and high concentrations and above it at intermediate concentrations. The deviation from GHK is seen more clearly when P_{Ca}/P_{Cs} is quantified for individual Ca²⁺ concentrations (Fig. 8 *B*). Around physiological concentrations of Ca²⁺ (1 and 1.8 mM), P_{Ca}/P_{Cs} shows a peak of 6.2 and 6.1, respectively. On the other hand, P_{Ca}/P_{Cs} is reduced to 2.6 in 110 and to 2.2 in 0.18.

The decrease in P_{Ca}/P_{Cs} at low concentrations of Ca²⁺ was surprising. It is not due to differences in activity coefficients that varied little due to the presence of the positively charged NMDG (see MATERIALS AND METHODS). An alternative explanation is that NMDG binds to Ca²⁺, reducing its effective concentration. However, P_{Ca}/P_{Cs} measured in 0.18 mM Ca²⁺ in 140 mM tetramethylammonium (TMA) ($P_{Ca}/P_{Cs} = 2.2 ± 0.2$, $n = 6$) was indistinguishable from that measured in 140 mM NMDG ($P_{Ca}/P_{Cs} = 2.2 ± 0.1$, $n = 7$), requiring that if NMDG binds to Ca²⁺, then TMA must do so to
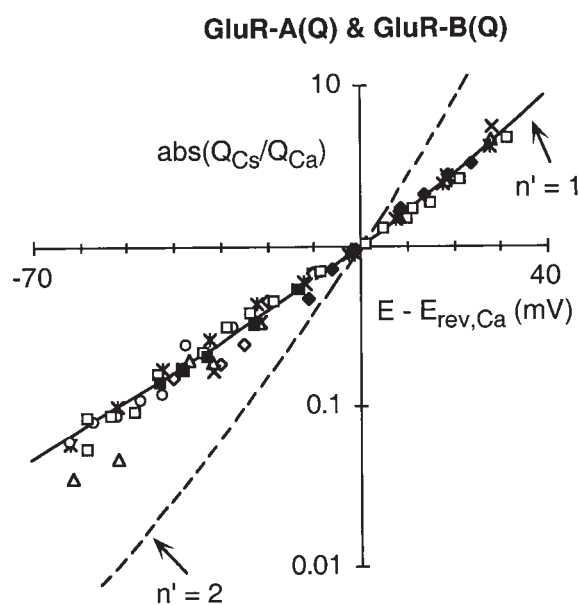
GluR-A(Q) & GluR-B(Q)

FIGURE 7. Biionic flux ratios in Ca²⁺-permeable AMPAR channels. Absolute of the biionic flux ratio, Q_{Cs}/Q_{Ca}, in GluR-A(Q) (*open symbols*) or GluR-B(Q) (*solid symbols*) AMPAR channels measured in 10 mM CaCl₂ in 140 mM NMDG. Values are plotted relative to the reversal potential ($E − E_{rev,Ca}$) as in Fig. 5. The absolute $E_{rev,Ca}$ was ∼−30 mV. The dashed line is Eq. 5 with $n' = 2$, which was found for NMDAR channels under the same ionic conditions (see Fig. 5 *A*). Total number of cells tested was: seven GluR-A(Q) and three GluR-B(Q).
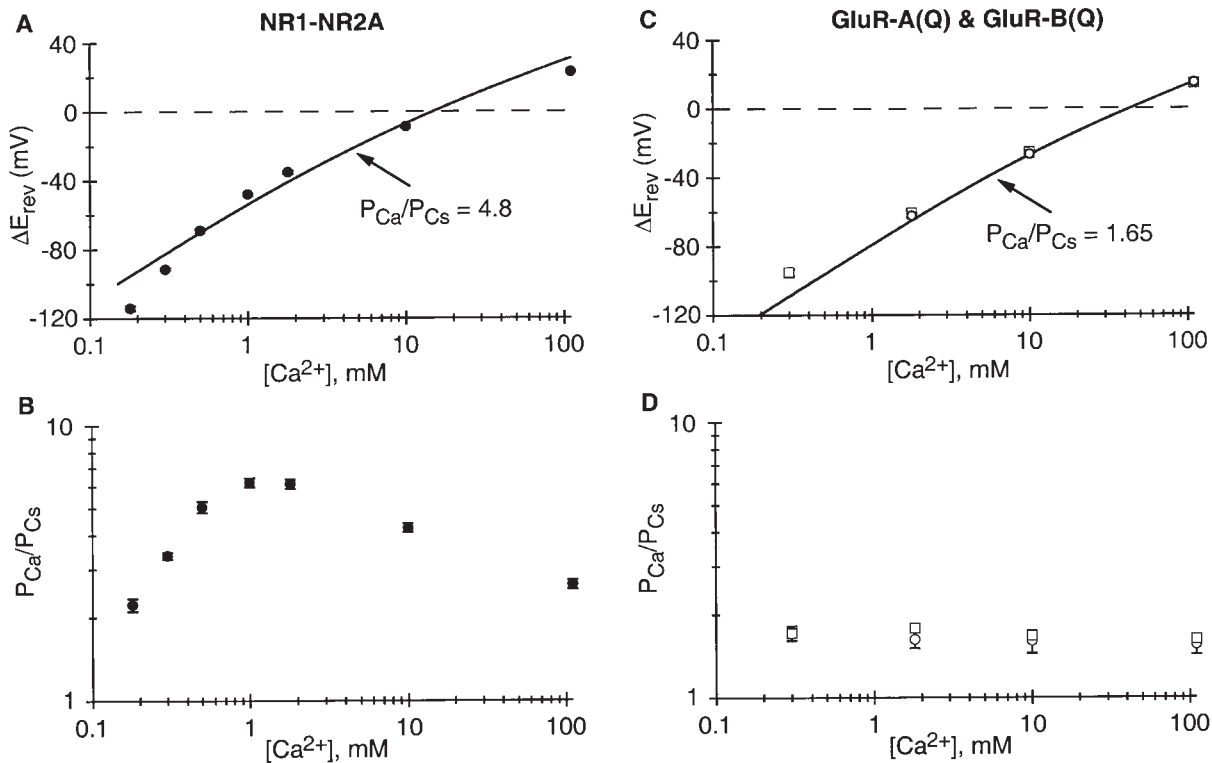
FIGURE 8. Ca^{2+} permeability in NR1-NR2A NMDAR but not Ca^{2+}-permeable AMPAR channels is concentration dependent. (*A*) Average change ($\pm$2*SEM) in the reversal potential, ΔE_{rev}, on replacing the high CsCl solution with a Ca^{2+}-containing solution (in 140 mM NMDG except for 110 mM Ca^{2+}). The continuous line is derived using the GHK equation (Iino et al., 1990):

$$\Delta E_{rev} = \frac{RT}{F}\ln\left[\frac{1}{2}\left(-1 + \sqrt{1 + 16\frac{P_{Ca}}{P_{Cs}}\frac{[Ca^{2+}]_0}{[Cs^+]_0}}\right)\right].$$

(*B*) Mean P$_{Ca}$/P$_{Cs}$ for individual Ca^{2+} concentrations derived from average changes in reversal potentials (shown in *A*) using the Lewis equation (Eq. 8). (*C* and *D*) Average change ($\pm$2*SEM) in the reversal potential ΔE_{rev} (*C*) and mean P$_{Ca}$/P$_{Cs}$ (*D*) for GluR-A(Q) ($\bigcirc$) and GluR-B(Q) ($\square$) AMPAR channels. Values displayed and analyzed as in *A* and *B*. In *C*, the deviation from the line at negative potentials reflects primarily that NMDG is weakly permeant in AMPAR channels. This permeability has been corrected for in *D* starting with Eq. 7 and assuming P$_{NMDG}$/P$_{Cs}$ = 0.02 [GluR-A(Q)] or 0.01 [GluR-B(Q)] (see MATERIALS AND METHODS). The derived P$_{Ca}$/P$_{Cs}$ at 1.8 or 10 mM [Ca^{2+}]$_0$ is altered only weakly when assuming a P$_{NMDG}$/P$_{Cs}$ of 0 or 0.02, whereas the value at 0.3 mM [Ca^{2+}]$_0$ is strongly altered and must be viewed cautiously. For this reason, P$_{Ca}$/P$_{Cs}$ in 0.3 mM [Ca^{2+}]$_0$ was not recorded in GluR-A(Q) channels, which would be dominated by the NMDG permeability.

the same extent. It also cannot be due to NMDG permeating the channel or contaminating concentrations of Ca^{2+}, both of which would lead to smaller changes in ΔE_{rev} (i.e., larger P$_{Ca}$/P$_{Cs}$s). Hence, the decrease in P$_{Ca}$/P$_{Cs}$ at low concentrations in NMDAR channels appears to be a property of the channel.

Fig. 8, *C* and *D*, shows the comparable measurement of Ca^{2+} permeability over a wide concentration range in AMPAR channels composed of GluR-A(Q) ($\bigcirc$) or GluR-B(Q) ($\square$) subunits. In Fig. 8 *C*, the smooth curve, derived using the GHK equation and assuming a P$_{Ca}$/P$_{Cs}$ of 1.65, describes the changes in reversal potential quite well in 1.8–110 mM Ca^{2+}. The change in the reversal potential in 0.3 mM Ca^{2+}, however, was not as large as expected. Nevertheless, NMDG is weakly permeant in these channels (see MATERIALS AND METH-

ODS). Indeed, when corrected for this weak NMDG permeability, P$_{Ca}$/P$_{Cs}$ shows essentially no concentration dependence over the entire concentration range (Fig. 8 *D*).

In summary, Ca^{2+} permeability ratios in NMDAR channels depend strongly on Ca^{2+} concentration, indicating a deviation from GHK. In contrast, Ca^{2+}-permeable AMPAR channels do not show concentration-dependent permeability ratios. These results are consistent with the results of the biionic flux-ratio measurements.

Differences in Ca^{2+} Permeability between NMDAR and Ca^{2+}-permeable AMPAR Are Not Due to the Q/R/N Site

A structural determinant of Ca^{2+} influx in GluR channels is the amino acid residue located at the function-

GluR-B(N)

A

abs(Q_{Cs}/Q_{Ca})

$E - E_{rev,Ca}$ (mV)

n' = 1

n' = 2
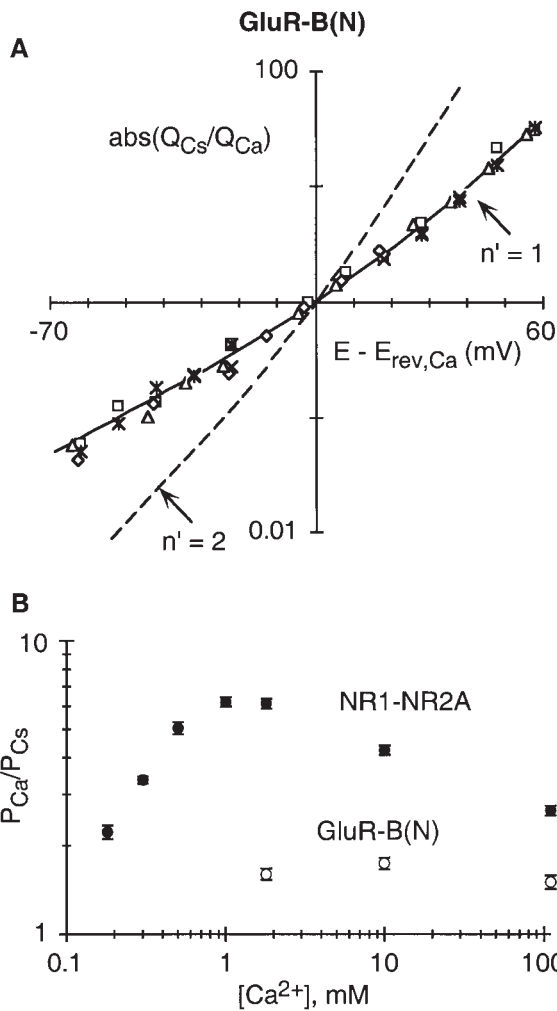
B

P_{Ca}/P_{Cs}

NR1-NR2A

GluR-B(N)

[Ca^{2+}], mM

FIGURE 9. An asparagine at the Q/R site in GluR-B channels does not alter its Ca^{2+} permeation properties. (A) Absolute of the biionic flux ratio, Q_{Cs}/Q_{Ca}, in GluR-B(N) AMPAR channels measured in 10 mM $CaCl_2$ in 140 mM NMDG. Values are plotted relative to the reversal potential ($E - E_{rev,Ca}$) as in Fig. 5. The absolute $E_{rev,Ca}$ was $\sim$−30 mV. A total of five cells were tested. (B) Mean P_{Ca}/P_{Cs} derived from average changes in the reversal potential (data not shown) for GluR-B(N) AMPAR channels. Values displayed and analyzed as in Fig. 8. NMDG was assumed to be impermeant in GluR-B(N) channels (see MATERIALS AND METHODS).

paragine at the N site in NMDAR channels] since this substitution has profound effects on channel gating (Schneggenburger and Ascher, 1997; see DISCUSSION).

Fig. 9 *A* shows the biionic flux ratio for GluR-B(N) channels in 10 mM [Ca^{2+}]$_o$. Because these channels were not blocked by intracellular polyamines, the biionic flux ratio could be determined at potentials at least 60 mV positive to $E_{rev,Ca}$. Like GluR-A(Q) and GluR-B(Q) channels, GluR-B(N) channels showed a biionic flux-ratio exponent of 1 between −60 and +60 mV of the reversal potential. Further, P_{Ca}/P_{Cs} in GluR-B(N) channels (Fig. 9 *B*, ○) also showed no concentration dependence. Hence, the biionic flux-ratio exponent of 1 and concentration-independent permeability ratios in GluR-B(N) suggest that the difference between NMDAR channels and Ca^{2+}-permeable AMPAR channels is not due to the composition of the Q/R site.

Table I compares fractional Ca^{2+} currents (P_f) in NMDAR channels and various subtypes of Ca^{2+}-permeable AMPAR channels, including GluR-B(N) at −60 mV. In comparison to GluR-B(Q) ($P_f \approx 4.0\%$), the fractional Ca^{2+} current in GluR-B(N) channels is somewhat higher, $\sim$4.7%. Nevertheless, this value remains considerably below that in NMDAR channels, which is $\sim$13.3%. Thus, an asparagine at the Q/R site does not yield AMPAR channels with fractional Ca^{2+} currents comparable with those in NMDAR channels.

DISCUSSION

Previously, flux ratios have been measured in K^+ and Na^+ channels using a radioactive tracer on one side of the membrane to distinguish between unidirectional fluxes (see INTRODUCTION). Using a combination of whole-cell current recordings and Ca^{2+} fluorescence measurements with intracellular Cs^+ and extracellular Ca^{2+} as the only permeant ions, we quantified unidirectional fluxes in NMDAR and Ca^{2+}-permeable AMPAR channels over a wide voltage range. A similar approach to quantifying unidirectional fluxes could be used in other classes of channels that have a mixed Ca^{2+} and monovalent permeability, such as nicotinic AChR and

ally critical Q/R/N site in the pore-lining M2 segment (Hollmann and Heinemann, 1994). Ca^{2+}-permeable AMPAR channels have a glutamine (Q) at this site, whereas NMDAR channels have an asparagine (N). To test whether the composition of the Q/R/N site underlies the difference between NMDAR and Ca^{2+}-permeable AMPAR channels, we measured biionic flux ratios, the concentration dependence of reversal potentials, and fractional Ca^{2+} currents in GluR-B(N) channels (Fig. 9 and Table I). This mutant Ca^{2+}-permeable AMPAR channel has an asparagine (N) substituted at the Q/R site (Burnashev et al., 1992a). We did not test the reverse mutant [glutamine (Q), substituted for the as-

cGMP-gated channels (Rogers and Dani, 1995; see Table II in Neher, 1995).

Biionic Flux Ratios in NMDAR but Not in Ca^{2+}-permeable AMPAR Channels Deviate from the Prediction of GHK

The biionic flux ratio in NMDAR channels showed a clear deviation from the predictions of the GHK current equation, requiring a biionic flux-ratio exponent of $\sim$2 in 10 mM and 1.9 in 1.8 mM $[Ca^{2+}]_o$ (Fig. 5). In contrast, AMPAR channels, composed either of GluR-A(Q), -B(Q), or -B(N) subunits, did not show such a deviation, having a biionic flux-ratio exponent of 1 over a wide potential range (Figs. 7 and 9). The most basic conclusion from these results is that the mechanism of Ca^{2+} transport in NMDAR and AMPAR channels is different, apparently being more complex in NMDAR channels. The results for AMPAR channels also act as an internal control, arguing against calibration or activity problems.

NMDAR channels had a biionic flux-ratio exponent of $\sim$2. For Ussing type flux-ratio exponents, such behavior has been termed flux coupling and has been interpreted to reflect that the movement of ions across the pore does not occur independently (Hodgkin and Keynes, 1955). Further, for a variety of permeation models, including those based on absolute reaction (Eyring) rate theory, the absolute value of the biionic flux-ratio exponent reflects the minimum number of ions that can occupy the permeation pathway (see references in Hille, 1992; Stampe and Begenisich, 1996). At present, the interpretation of the biionic flux-ratio exponent is ambiguous. In part, this ambiguity arises because we used different ions on the opposite sides of the membrane, and whether these ions interact with the same or different sites in the pore is unknown. Nevertheless, although the mechanistic interpretation of the biionic flux-ratio exponent remains limited, this approach to quantifying biionic flux ratios, in combination with mutagenesis of functional residues, will provide insights into how ions interact with the pore over a wide voltage range.

In AMPAR channels, which have a smaller fractional Ca^{2+} current (Table I), the biionic flux-ratio exponent was $\sim$1, whereas in NMDAR channels, which have a nearly fourfold higher fractional Ca^{2+} current, it was $\sim$2, suggesting that this biionic flux-ratio exponent in NMDAR channels reflects the same properties of the channel that underlie their higher fractional Ca^{2+} currents. Recently, analyzing the block of wild-type and mutant NMDAR channels by extracellular Ca^{2+}, Premkumar and Auerbach (1996) identified a high affinity site for Ca^{2+} in the outer vestibule. The molecular identity of this external site remains as yet unidentified. Nevertheless, it senses little of the transmembrane electric field and is distinct from the N-site asparagines,

which are positioned at or near the channel's narrow constriction (Wollmuth et al., 1996; see also Sharma and Stevens, 1996), a structure located $\sim$50–60% across the transmembrane electric field (Villarroel et al., 1995; Zarei and Dani, 1995). Thus, the deviation from GHK in NMDAR channels may reflect that Ca^{2+} interacts with multiple sites in the pore: the N-site asparagines positioned at the channel's narrow constriction and an additional site putatively positioned externally, probably <10% across the field. Identifying this putative external site will allow a direct test of the relationship between this external site, fractional Ca^{2+} currents, and biionic flux ratios.

The GHK current equation is derived assuming independence of ion movement and a constant transmembrane electric field. A biionic flux-ratio exponent of 1 is consistent with the predictions of GHK current equation, but does not necessarily indicate that the ions in the pore follow the assumptions of this test since, even in the simpler case of the Ussing flux-ratio exponent, it can also arise in single ion pores (Hille, 1992), when the transmembrane electric field is not constant (Chen and Eisenberg, 1993), or in multi-ion pores with distinct energetic profiles (Begenisich and Busath, 1981). Indeed, AMPAR channels do show deviations from GHK (Burnashev et al., 1995) and ion–ion interactions in the pore (Bahring et al., 1997). Nevertheless, a possible explanation for the biionic flux-ratio exponent of 1 in AMPAR channels is that these channels lack the putative external site present in NMDAR channels and that the mechanism of Ca^{2+} transport in them is dominated by a single site, possibly the amino acid side chains occupying the Q/R site.

Differences in Ca^{2+} Permeability between GluR Subtypes Are Not Due to the Q/R/N Site

The amino acid residue occupying the Q/R/N site is an important determinant of Ca^{2+} transport in both NMDAR and AMPAR channels. This site, however, is not responsible for the quantitative difference in Ca^{2+} transport between these GluR subtypes since fractional Ca^{2+} currents in GluR-B(N) channels were comparable with those in GluR-B(Q) rather than in NMDAR channels (Table I). The reverse substitution in NMDAR channels (glutamine at the N-site) does lead to reduced fractional Ca^{2+} currents (L.P. Wollmuth, unpublished data). However, the interpretation of this mutant channel in terms of its permeation properties is complex because of multiple subconductance states with different permeation properties (Schneggenburger and Ascher, 1997). Also, these mutant NMDAR channels are more strongly blocked by extracellular Ca^{2+} than wild-type NMDAR channels (Premkumar and Auerbach, 1996), an effect opposite that seen in AMPAR channels.

NMDAR Channels Have Concentration-dependent Permeability Ratios

In NMDAR channels, P_{Ca}/P_{Cs} showed a maximum between 1 and 1.8 mM Ca^{2+} and was reduced at both higher and lower concentrations (Fig. 8, *A* and *B*). These concentration-dependent permeability ratios are presumably a manifestation of the same properties of the channel that underlie the deviation of the biionic flux ratios from GHK. If this is true, then surface charges do not seem to play a prominent role in Ca^{2+} transport in NMDAR channels since reversal potentials showed a downward deflection at very low concentrations in contrast to an upward deflection expected for surface charges. This conclusion is consistent with that of Zarei and Dani (1994).

Previous measurements of the concentration dependence of reversal potentials in GluR channels show similarities and differences from our measurements. Reversal potentials in native NMDAR and Ca^{2+}-permeable AMPAR channels have been measured using a pure Ca^{2+} extracellular solution similar to what we used (Iino et al., 1990; Koh et al., 1995*b*). For NMDAR channels, the reversal potentials were indistinguishable from our measurements and showed a similar deviation from GHK. The main difference from our work is that we tested a much wider concentration range of Ca^{2+}, where the deviation from GHK was more pronounced. For native AMPAR channels, it is difficult to quantitatively compare the results since a small amount of edited GluR-B(R) may be present, shifting negative the reversal potentials. Nevertheless, the relationship between measured reversal potentials and the fitted GHK equation shows less deviation than in NMDAR channels. The deviation disappears when P_{Ca}/P_{Cs} is corrected for the small NMDG permeability present in AMPAR channels (Burnashev et al., 1996) (compare Fig. 8, *C* and *D*).

Another approach to test for concentration dependence of Ca^{2+} permeability has been to record changes in reversal potentials on switching from a high extracellular monovalent solution with no added Ca^{2+} to the same solution with added Ca^{2+} (Jahr and Stevens, 1993; Zarei and Dani, 1994; Schneggenburger, 1996; L.P. Wollmuth, unpublished data). In these instances, any deviation from GHK is negligible. In addition, many channel types that contain multiple permeant ions show a paradoxical behavior in mixtures of permeant ions, where the conductance or reversal potential of currents passes through a minimum rather than changing monotonically. This anomalous mole fraction dependence is a property of channel models with more than one ion at a time in the single-file region of the pore (Hille, 1992). Neither NMDAR (Zarei and Dani, 1994) nor kainate receptor (Gu and Huang, 1991) channels show this effect (but see Mayer and Westbrook, 1987). The result for kainate receptor channels is in agreement with our results for AMPAR channels. However, the basis for the lack of a clear anomalous mole fraction effect in NMDAR channels is unknown, but its absence suggests that, while there may be multiple sites in the pore of NMDAR channels for permeating ions, these sites are not multiply occupied.

Conclusion

Activation of NMDAR and Ca^{2+}-permeable AMPAR channels mediates post-synaptic Ca^{2+} influx. Functionally, Ca^{2+} transport differs in these channels in that it is nearly fourfold higher in NMDAR than in Ca^{2+}-permeable AMPAR channels. This difference arises because the mechanism of Ca^{2+} transport in these channels is different, possibly reflecting the presence of an additional external site for Ca^{2+} in NMDAR channels that is absent in AMPAR channels.

REFERENCES

Bahring, R., D. Bowie, M. Benveniste, and M.L. Mayer. 1997. Permeation and block of rat GluR6 glutamate receptor channels by internal and external polyamines. *J. Physiol. (Lond.).* 502:575–589.

Begenisich, T., and D. Busath. 1981. Sodium flux ratio in voltage-clamped squid giant axons. *J. Gen. Physiol.* 77:489–502.

Begenisich, T., and P. De Weer. 1980. Potassium flux ratio in voltage-clamped squid giant axons. *J. Gen. Physiol.* 76:83–98.

Benos, D.J., B.A. Hyde, and R. Latorre. 1983. Sodium flux ratio through the amiloride-sensitive entry pathway in frog skin. *J. Gen.*

Physiol. 81:667–685.

Bliss, T.V.P., and G.L. Collingridge. 1993. A synaptic model of memory: long-term potentiation in the hippocampus. *Nature.* 361:31–39.

Bowie, D., and M.L. Mayer. 1995. Inward rectification of both AMPA and kainate subtype glutamate receptors generated by polyamine-mediated ion channel block. *Neuron.* 15:453–462.

Burnashev, N. 1996. Calcium permeability of glutamate-gated channels in the central nervous system. *Curr. Opin. Neurobiol.* 6:311–

317.

Burnashev, N., H. Monyer, P.H. Seeburg, and B. Sakmann. 1992*a*. Divalent ion permeability of AMPA receptor channels is dominated by the edited form of a single subunit. *Neuron.* 8:189–198.

Burnashev, N., R. Schoepfer, H. Monyer, J.P. Ruppersberg, W. Günther, P.H. Seeburg, and B. Sakmann. 1992*b*. Control by asparagine residues of calcium permeability and magnesium blockade in the NMDA receptor. *Science.* 257:1415–1419.

Burnashev, N., A. Villarroel, and B. Sakmann. 1996. Dimensions and ion selectivity of recombinant AMPA and kainate receptor channels and their dependence on Q/R site residues. *J. Physiol. (Lond.).* 496:165–173.

Burnashev, N., Z. Zhou, E. Neher, and B. Sakmann. 1995. Fractional calcium currents through recombinant GluR channels of the NMDA, AMPA and kainate receptor subtypes. *J. Physiol. (Lond.).* 485:403–418.

Chen, D., and R. Eisenberg. 1993. Charges, currents, and potentials in ionic channels of one conformation. *Biophys. J.* 64:1405–1421.

Choi, D.W. 1988. Glutamate neurotoxicity and diseases of the nervous system. *Neuron.* 1:623–634.

Grynkiewicz, G., M. Poenie, and R.Y. Tsien. 1985. A new generation of Ca^{2+} indicators with greatly improved fluorescence properties. *J. Biol. Chem.* 260:3440–3450.

Gu, Y., and L.-T.M. Huang. 1991. Block of kainate receptor channels by Ca^{2+} in isolated spinal trigeminal neurons of rat. *Neuron.* 6:777–784.

Hille, B. 1992. Ionic Channels of Excitable Membranes. 2nd ed. Sinauer Associates, Inc., Sunderland, MA. 607 pp.

Hodgkin, A.L., and R.D. Keynes. 1955. The potassium permeability of a giant nerve fibre. *J. Physiol. (Lond.).* 128:61–88.

Hollmann, M., M. Hartley, and S. Heinemann. 1991. Ca^{2+} permeability of KA-AMPA-gated glutamate receptor channels depends on subunit composition. *Science.* 252:1028–1031.

Hollmann, M., and S. Heinemann. 1994. Cloned glutamate receptors. *Annu. Rev. Neurosci.* 17:31–108.

Horowicz, P., P.W. Gage, and R.S. Eisenberg. 1968. The role of the electrochemical gradient in determining potassium fluxes in frog striated muscle. *J. Gen. Physiol.* 51:193s–203s.

Hume, R.I., R. Dingledine, and S.F. Heinemann. 1991. Identification of a site in glutamate receptor subunits that controls calcium permeability. *Science.* 253:1028–1031.

Iino, M., S. Ozawa, and K. Tsuzuki. 1990. Permeation of calcium through excitatory amino acid receptor channels in cultured rat hippocampal neurones. *J. Physiol. (Lond.).* 424:151–165.

Jahr, C.E., and C.F. Stevens. 1993. Calcium permeability of the *N*-methyl-D-aspartate receptor channel in hippocampal neurons in culture. *Proc. Natl. Acad. Sci. USA.* 90:11573–11577.

Koh, D.-S., N. Burnashev, and P. Jonas. 1995*a*. Block of native Ca^{2+}-permeable AMPA receptors in rat brain by intracellular polyamines generates double rectification. *J. Physiol. (Lond.).* 486:305–312.

Koh, D.-S., J.R. Geiger, P. Jonas, and B. Sakmann. 1995*b*. Ca^{2+}-permeable AMPA and NMDA receptor channels in basket cells of rat hippocampal dentate gyrus. *J. Physiol. (Lond.).* 485:383–402.

Lewis, C.A. 1979. Ion-concentration dependence of the reversal potential and the single channel conductance of ion channels at the frog neuromuscular junction. *J. Physiol. (Lond.).* 286:417–445.

MacDermott, A.B., M.L. Mayer, G.L. Westbrook, S.J. Smith, and J.L. Barker. 1986. NMDA receptor activation increases cytoplasmic calcium concentration in cultured spinal cord neurones. *Nature.* 321:261–263.

Mayer, M.L., and G.L. Westbrook. 1987. Permeation and block of *N*-methyl-D-aspartic acid receptor channels by divalent cations in mouse cultured central neurones. *J. Physiol. (Lond.).* 394:501–527.

Monyer, H., N. Burnashev, D.J. Laurie, B. Sakmann, and P.H. Seeburg. 1994. Developmental and regional expression in the rat brain and functional properties of four NMDA receptors. *Neuron.* 12:529–540.

Neher, E. 1995. The use of fura-2 for estimating Ca buffers and Ca fluxes. *Neuropharmacology.* 34:1423–1442.

Premkumar, L.S., and A. Auerbach. 1996. Identification of a high affinity divalent cation binding site near the entrance of the NMDA receptor channel. *Neuron.* 16:869–880.

Rogers, M., and J.A. Dani. 1995. Comparison of quantitative calcium flux through NMDA, ATP, and ACh receptor channels. *Biophys. J.* 68:501–506.

Schneggenburger, R. 1996. Simultaneous measurement of Ca^{2+} influx and reversal potentials in recombinant *N*-methyl-D-aspartate receptor channels. *Biophys. J.* 70:2165–2174.

Schneggenburger, R., and P. Ascher. 1997. Coupling of permeation and gating in an NMDA-channel pore mutant. *Neuron.* 18:167–177.

Schneggenburger, R., Z. Zhou, A. Konnerth, and E. Neher. 1993. Fractional contribution of calcium to the cation current through glutamate receptor channels. *Neuron.* 11:133–143.

Seeburg, P.H. 1993. The TINS/TiPS Lecture. The molecular biology of mammalian glutamate receptor channels. *Trends Neurosci.* 16:359–365.

Sharma, G., and C.F. Stevens. 1996. Interactions between two divalent ion binding sites in *N*-methyl-D-aspartate receptor channels. *Proc. Natl. Acad. Sci. USA.* 93:14170–14175.

Stampe, P., and T. Begenisich. 1996. Unidirectional K+ fluxes through recombinant *Shaker* potassium channels expressed in single *Xenopus* oocytes. *J. Gen. Physiol.* 107:449–457.

Ussing, H.H. 1949. The distinction by means of tracers between active transport and diffusion. *Acta Physiol. Scand.* 19:43–56.

Vestergaard-Bogind, B., P. Stampe, and P. Christophersen. 1985. Single-file diffusion through the Ca^{2+}-activated K+ channel of human red cells. *J. Membr. Biol.* 88:67–75.

Villarroel, A., N. Burnashev, and B. Sakmann. 1995. Dimensions of the narrow portion of a recombinant NMDA receptor channel. *Biophys. J.* 68:866–875.

Wollmuth, L.P., T. Kuner, P.H. Seeburg, and B. Sakmann. 1996. Differential contribution of the NR1- and NR2A-subunits to the selectivity filter of recombinant NMDA receptor channels. *J. Physiol. (Lond.).* 491:779–797.

Zarei, M.M., and J.A. Dani. 1994. Ionic permeability characteristics of the *N*-methyl-D-aspartate receptor channel. *J. Gen. Physiol.* 103:231–248.

Zarei, M.M., and J.A. Dani. 1995. Structural basis for explaining open-channel blockade of the NMDA receptor. *J. Neurosci.* 15:1446–1454.